Ocean Modelling 52–53 (2012) 69–75

Contents lists available at SciVerse ScienceDirect

Ocean Modelling

journal homepage: www.elsevier.com/locate/ocemod

Three-dimensional characterization and tracking of an Agulhas Ring

Gary Froyland [a], Christian Horenkamp [b,*], Vincent Rossi [a], Naratip Santitissadeekorn [a,1], Alex Sen Gupta [c]

[a] School of Mathematics and Statistics, University of New South Wales, Sydney, NSW 2052, Australia
[b] Department of Mathematics, University of Paderborn, 33098 Paderborn, Germany
[c] Climate Change Research Centre, University of New South Wales, Sydney, NSW 2052, Australia

ARTICLE INFO

Article history:
Received 27 November 2011
Received in revised form 5 May 2012
Accepted 11 May 2012
Available online 27 May 2012

Keywords:
Oceanic eddies
Agulhas Rings
Agulhas leakage
Transition matrix
Coherent pairs
Lagrangian three-dimensional oceanic eddy

ABSTRACT

A novel probabilistic methodology is applied to identify optimally coherent structures associated with Agulhas Rings, within a time varying velocity field in the South Atlantic Ocean, as simulated by an eddy-permitting ocean general model. It is shown that this technique provides a way of identifying the three-dimensional shape of a particular Ring in the upper ocean and tracking its evolution over space and time. Based on this three-dimensional representation we can accurately measure the amount of water mass remaining in an Agulhas Ring over time and consequently how much heat or salt is released from the structure as it decays. Identification techniques based on relative vorticity or the Okubo-Weiss parameter have previously been developed for a surface snapshot. Extending these methods in the vertical direction in the upper ocean and comparing the decay of all three-dimensional structures obtained by different methods, we demonstrate that our technique is able to define structures that are more coherent over time than classical methods. While our investigation concentrates on a single Agulhas Ring located in the Cape-Basin from May 2000 over 6 months, the technique may be extended to examine multiple Rings and other coherent structures that are involved in the Agulhas leakage.

1. Introduction

The Agulhas circulation around southern Africa plays a key role in the climate system via its effects on the global ocean circulation (see a review by Beal et al. (2011) and references therein). The transport of warm saline waters from the Indian Ocean into the upper Atlantic Ocean provides closure for the global overturning circulation (Weijer et al., 2002). This transport is effected by a number of processes including the advection of large anticyclonic eddies or Agulhas Rings that detach periodically at the Agulhas current retroflection, smaller cyclonic eddies, filaments and a mean circulation (De Ruijter et al., 1999; Lutjeharms, 2006; Doglioli et al., 2006). How much heat and salt an Agulhas Ring transports, and how far into the North Atlantic the Ring transports these tracers, is sensitive to how long the water remains within a Ring as well as its path (Treguier et al., 2003).

Several approaches have been developed to identify and spatially define an eddy at the ocean surface. Physical criteria require the calculation of dynamical properties at the surface, and eddies are identified where a given threshold of these properties is exceeded. Dynamical properties of the flow field that have been used to identify eddies include sea-level anomaly (SLA) magnitude (Isern-Fontanet et al., 2003; Treguier et al., 2003), relative vorticity (RV) (van Sebille et al., 2010), the Okubo-Weiss (OW) parameter (Isern-Fontanet et al., 2003; Chaigneau et al., 2008), the gradient tensor, which combines the previous techniques (Morrow et al., 2004) or more sophisticated techniques such as wavelet analysis of relative vorticity maps (Doglioli et al., 2007). Other techniques use the geometry of the flow to locate an eddy. Sadarjoen and Post (2000) were among the first to use streamline function curvatures and a winding-angle (WA) detection algorithm to detect mesoscale eddies. This was then applied by Chaigneau et al. (2008) over the south eastern Pacific and compared to the OW parameter. In their study, the WA method detected mesoscale eddies more accurately than the OW parameter. The recent study by Chelton et al. (2011), reviews all current techniques and proposed a new SSH-based automated criteria. Their techniques has the advantage of being threshold-free, thus allowing its application to the global ocean. The detection of Agulhas Rings by all the above methods revealed slightly different results, which can be evaluated by comparing the number of real or spurious structures identified (Chaigneau et al., 2008). However they are all based on surface data fields. In order to estimate properties associated with the *three-dimensional* structure of the rings, including an estimation of its internal volume, most authors simply extended the surface edges of the eddy to a given depth along the vertical to make further calculations (e.g. De Ruijter et al., 1999; Treguier et al., 2003). To estimate the volume of an eddy, Richardson (2007) examined the perfect cylinder theory as well as the truncated inverted cone alternative.

* Corresponding author. Tel.: +49 5251 60 4209.
E-mail address: horenc@math.upb.de (C. Horenkamp).
[1] Current address: Department of Mathematics, UNC-CH, CB 3250, Phillips Hall, Chapel Hill, NC 27599-3250, USA.

1463-5003/$ - see front matter © 2012 Elsevier Ltd. All rights reserved.
http://dx.doi.org/10.1016/j.ocemod.2012.05.001

Based on in-situ data analysis (tangential velocities, hydrodynamic signatures), van Aken et al. (2003) pointed out the high variability that exists in the vertical extension of these structures. Hence a rigorous three-dimensional characterization of each eddy is needed to better estimate its decay and the associated inter-basin leakage due to the Agulhas Rings.

The rate of Agulhas Ring decay has also been the subject of a number of previous studies; e.g. (Byrne et al., 1995; Schouten et al., 2000; Treguier et al., 2003; de Steur et al., 2004; Richardson, 2007; van Sebille et al., 2010). These are based on, for instance, the time evolution of the SSH field (Byrne et al., 1995), in situ data and drifter trajectories (van Aken et al., 2003; Richardson, 2007), modeled passive tracers (de Steur et al., 2004), transport estimation from a global OGCM (Treguier et al., 2003), modeled Lagrangian float trajectories, and the evolution of relative vorticity (van Sebille et al., 2010). Although these studies used different approaches, they all showed a significant decay of the ring from its formation region in the south Atlantic Ocean. The bathymetric erosion effect was studied by Schouten et al. (2000) and Treguier et al. (2003), but they reported that it is not a dominant mechanism. Using hydrographic sections, van Aken et al. (2003) presented observational evidence of the exchange of water from the eddy core with its surroundings. de Steur et al. (2004) showed that a Ring forming filamental structures that mix with surrounding water causes a loss of tracer from the eddy. They also studied the vertical structure of the ring and found that the eddy was less coherent at greater depth: the decay of tracer content in the thermocline shows that in the first months up to 40% of the ring water is expelled whereas it is up to 90% in deeper layers. Richardson (2007), using real ocean floats to study Agulhas leakage, discussed the effect of the path taken by the rings and their associated transport. More recently van Sebille et al. (2010) showed a very fast decay of all anticyclonic rings inside the Cape-Basin. Depending on the numerous methods used, the literature contains highly varying estimates of Agulhas leakage due to rings, ranging from around 3–9 Sv (Richardson, 2007).

In prior work, Agulhas Rings have been analyzed using Eulerian methods such as SLA, OW, RV and SSH (Isern-Fontanet et al., 2003). Other studies focussing on the decay of the rings used more appropriate Lagrangian approaches (e.g. van Sebille et al., 2010). We also adopted a Lagrangian perspective to tackle the challenging problem of detecting an eddy and quantifying its coherence over time in a full three-dimensional framework. Lagrangian methods are specially suited to study transport properties in a geophysical fluid and to delineate fluid domains with distinct dynamical characteristics. In this work, we apply a new approach that identifies oceanic regions that are optimally coherent over a fixed time span (i.e. water masses that remain intact with little loss to the outside). More precisely, we identify pairs of geometrically regular regions (A, B) within the oceanic domain, that maximize the probability that a tracer starts in set A and terminates in set B after flowing for a fixed time-period. These maximally coherent structures will be used to define Agulhas Rings within the Cape-Basin. A series of publications (Froyland et al., 2008; Froyland et al., 2007; Dellnitz et al., 2009) have already successfully applied a similar approach to the (effectively nonautonomous) oceanic flow over short time periods to detect persistent and almost stationary structures such as the Weddell and Ross Gyres. In these studies, we identified subsets (e.g. geographical oceanic domain) of the Southern Ocean for which the probability that a tracer released in a subset remains in the same subset is maximized. A comparison with the SSH field showed strong correlation at the surface between maximally coherent structures and large eddies or gyres within the oceanic domain. To identify non-stationary maximally coherent structures over longer time intervals, we apply a novel transfer operator approach developed in Froyland et al. (2010). This approach was successfully applied to the stratospheric polar vortex. Here we used the approach of Froyland et al. (2010) in a subregion of the Cape-Basin containing an Agulhas Ring to calculate the most coherent three-dimensional objects over a 6 month period. The input data for this approach is the advection field from an eddy permitting ocean general circulation model (Barnier et al., 2006).

The outline of this paper is as follows: in Section 2 we describe the relationship between Agulhas Rings and *coherent pairs*. We provide in Section 3 a brief summary of the technique used for the identification of the Agulhas Rings, which we apply in Section 4. Our conclusions are presented in Section 5.

2. Nonautonomous oceanic flow and coherent pairs

We focus in a portion if the ocean, specifically $X = [8.5°\mathrm{E}, 13°\mathrm{E}] \times [36°\mathrm{S}, 32.5°\mathrm{S}] \times [0\ \mathrm{m}, -5126\ \mathrm{m}]$, which contains a single ring-like structure during May 2000. This region was chosen by visually examining the simulated sea surface height anomalies and selecting a region containing anomalous high sea-level in a ring structure. The flow of the ocean is described by a time-dependent ordinary differential equation

$$\frac{dx}{dt} = f(x(t), t), \tag{1}$$

where the vector field f is obtained from the output of the ORCA025 global ocean model (Barnier et al., 2006). The ORCA025 model was forced by historical surface fluxes based on satellite observations over the time period January 1958–December 2002 and outputs consist in 5-day averaged velocities on a grid with 0.25° resolution in longitude and latitude direction and with 46 non-uniform depth layers. The terminal point of a particle, initially at $x_0 \in \mathcal{X}$ at time t, after flowing time τ is given by $\phi(x_0, t, \tau)$, where $\mathcal{X}$ is the entire oceanic domain. Our initial domain X at time t is as given above and we denote the domain at the final time by $Y = \phi(X, t, \tau)$ (see Fig. 1).

The aim of this paper is to calculate pairs of equal volume ocean subregions A_t and $A_{t+\tau}$ with the property that the likelihood of a trajectory that begins in A_t at time t and finishes in $A_{t+\tau}$ at time $t+\tau$, is maximal. Thus, these two regions should satisfy $A_{t+\tau} \approx \phi(A_t, t, \tau)$. We can directly measure the amount of water mass which is transported from A_t to $A_{t+\tau}$ over the time τ by the so-called coherence ratio ρ, which is the ratio of the volume of water that successfully flows from A_t to $A_{t+\tau}$, to the initial volume of A_t:

$$\rho(A_t, A_{t+\tau}) := \frac{\mathrm{vol}(A_t \cap \phi(A_{t+\tau}, t+\tau, -\tau))}{\mathrm{vol}(A_t)}. \tag{2}$$

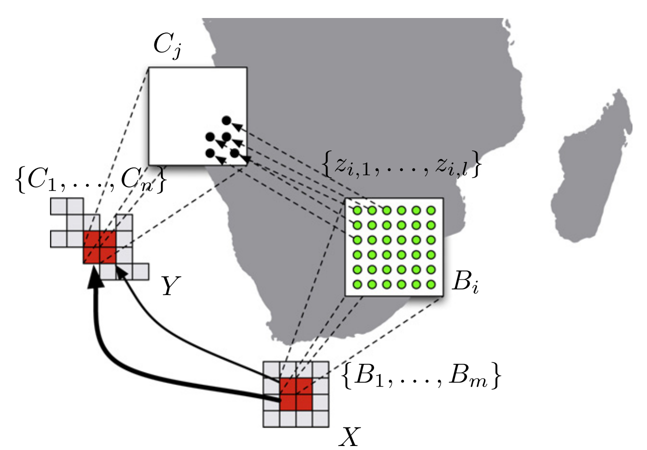

Fig. 1. Regions X and Y are divided into a matrix of boxes $\{B_1, \ldots, B_m\}$ and $\{C_1, \ldots, C_n\}$, respectively. Each box B_i is seeded with l Lagrangian particles $\{z_{i,1}, \ldots, z_{i,l}\}$ and advected forward in time. $P_{i,j}$, the probability of a particle starting in B_i and ending in C_j is simply the volume associated with the black particles divided by the volume associated with the green particles. (For interpretation of the references to colour in this figure legend, the reader is referred to the web version of this article.)

To detect Agulhas Rings, we look for pairs with maximized coherence. Leaving formal considerations until the following section, if $A_t^*, A_{t+\tau}^*$ are the pair of subregions maximizing $\rho(A_t, A_{t+\tau})$, then we identify A_t as the Agulhas ring location at time t and $A_{t+\tau}$ as the Agulhas ring location at time $t+\tau$. Maximizing coherence corresponds to minimal "leakage" of trajectories on their journey from A_t to $A_{t+\tau}$, resulting in coherent ring-like dynamical behavior.

3. Transition matrix approach

In order to compute maximally coherent subregions, we first build a transition matrix that describes a spatially discretised version of the Lagrangian flow dynamics. We form a grid of boxes $\{B_1, \ldots, B_m\}$ covering X and a grid of boxes $\{C_1, \ldots, C_n\}$ covering Y. To obtain conditional likelihoods of trajectories flowing from one box B_i at the initial time t to another box C_j at the final time $t+\tau$ we construct the transition matrix

$$\mathbf{P}_{t,\tau;i,j} := \frac{\mathrm{vol}(B_i \cap \phi(C_j, t+\tau, -\tau))}{\mathrm{vol}(B_i)}. \tag{3}$$

The entry $\mathbf{P}_{t,\tau;i,j}$ can be interpreted as the likelihood that a particle selected uniformly at random in B_i at time t will be in C_j at time $t+\tau$.

The entries $\mathbf{P}_{t,\tau;i,j}$ of (3) cannot be easily calculated directly and must be estimated numerically. To carry out this estimation, we release l Lagrangian particles $\{z_{i,r}\}_{r=1\ldots l}$ on a uniform subgrid of box B_i, $i = 1, \ldots, m$ and numerically integrate each $z_{i,r}$ from time t to $t+\tau$. We then count how many of these points fall in each box C_j, $j = 1, \ldots, n$ and assign conditional likelihoods $\mathbf{P}_{t,\tau;i,j}$ accordingly:

$$\tilde{\mathbf{P}}_{t,\tau;i,j} = \frac{\text{number of points } z_{i,r} \text{ with } z_{i,r} \in B_i \text{ and } \phi(z_{i,r}, t, \tau) \in C_j}{l}, \tag{4}$$

where $l =$ number of points $z_{i,r}$ in B_i as defined above. Fig. 1 presents a visualization of the approximation of the transition matrix.

To calculate the trajectories of the $z_{i,r}$ we use a standard Runge–Kutta approach with a time-step of 1 h and approximate $f(x(t), t)$ in (1) via a linear interpolation between two 5-day averaged velocity fields. At the end of each 5-day period of integration we apply a parameterization to account for the strong mixing within the upper ocean. The mixed layer depth (MLD) refers to a region of vigorous mixing close to the surface and is not captured by the velocity field provided by the model. For the implementation of the MLD we refer to Froyland et al. (2008), Dellnitz et al. (2009). Using 5-day output we applied our MLD parameterization every 5 days rather than every month as per Froyland et al., 2008.

Having constructed the transition matrix $\mathbf{P}_{t,\tau;i,j}$ we now outline our methodology to extract maximally coherent regions using spectral information. Details on the numerical methodology may be found in Froyland et al. (2010). Below we describe an algorithm that gives an overview of the main points.

We first define a few more relevant objects. For an ocean region $A \subset X$, we define $m_X(A) = \mathrm{vol}(A)/\mathrm{vol}(X)$, the fractional volume of X occupied by A, where $\mathrm{vol}(A)$ is the volume of the region A. The quantity $m_X(A)$ is simply the fractional volume of X occupied by A.

Algorithm 1 (*Construction of singular vectors*).

1. Define the row vector p of length m by $p_i = m_X(B_i)$, $i = 1, \ldots, m$. The vector p carries the fractional box volumes of boxes B.
2. Construct the row vector q of length n by matrix multiplication: $q = p\mathbf{P}_{t,\tau}$. The vector q carries the fractional box volumes assigned to the C_j, $j = 1, \ldots, n$ obtained by advecting forward the fractional box volumes given by p at time t to the final time $t+\tau$.
3. Construct the $m \times n$ matrix L as $L_{ij} = p_i \mathbf{P}_{t,\tau,i,j}/q_j$. The matrix L is a "normalized" version of $\mathbf{P}_{t,\tau}$ that satisfies $\mathbf{1}L = \mathbf{1}$, where $\mathbf{1}$ is a vector of 1s (this is obvious from the definition of L). We interpret this equation dynamically as a constant density (e.g. tracer concentration) on X, represented by the function $\mathbf{1}$, being mapped by L to a constant density on Y.
4. Let Π_p (resp. Π_q) be an $m \times m$ (resp. $n \times n$) diagonal matrix with p (resp.q) on the diagonal. Calculate the two largest singular values σ_1, σ_2 of the matrix $\Pi_p^{1/2}\mathbf{P}_{t,\tau}\Pi_q^{-1/2}$. By construction, $\sigma_1 = 1$ (and generically if the dynamics are "mixing", $\sigma_2 < 1$). If a coherent region is present, one should have $\sigma_2 \approx \sigma_1$.
5. Compute the left and right singular vectors corresponding to σ_2 (call them $\hat{x}$ and $\hat{y}$, respectively) and form $x = \hat{x}\Pi_p^{-1/2}$ and $y = \hat{y}\Pi_p^{-1/2}$.

The above singular vector computation solves a relaxation of a discrete "flow optimization" problem that tries to partition X and Y into two sets so that flow between each pair of sets is maximized; further details on the setting up of this optimization problem may be found in Froyland et al. (2010).

One can map the m entries of x to the m boxes B_i, $i = 1, \ldots, m$ to obtain an image like Fig. 3. Similarly, one can map the n entries of y to the n boxes C_j, $j = 1, \ldots, n$. The values of x and y could be interpreted as follows: in the "perfectly coherent" situation, one should see x take on two distinct values, one positive and the other negative; similarly for the entries of y. The spatial region corresponding to the positive values of x will indicate one maximally coherent set at time t, namely A_t, and the spatial region corresponding to the positive values of y will indicate the matching maximally coherent set at time $t+\tau$, namely $A_{t+\tau}$. The spatial regions corresponding to negative values of x and y indicate the remainder of X and Y, respectively; in fact, the x and y are unique only up to a change of sign, so it may be that negative values correspond to the coherent set of interest and positive values correspond to "the rest" of X and Y.

In the "not perfectly coherent" situation, one will not see such a sharp change in value in the entries of x and y from one constant value to another constant value. Rather, there will be a gradual shift from negative to positive values. Nevertheless, heuristically, sharp gradients are meaningful and one can often "eyeball" the coherent regions as those regions with mostly constant values surrounded by a sharp gradient. In order to find the best values of x and y to separate A_t and $A_{t+\tau}$ we employ a line search optimization procedure.

Algorithm 2 (*Thresholding of singular vectors*).

1. For some thresholds b and c, define $X(b) := \cup_{x_i > b} B_i$ and $Y(c) := \cup_{y_i > c} C_i$. In other words, $X(b)$ is the union of all boxes with corresponding x-values greater than the threshold b, and $Y(c)$ is the union of all boxes with corresponding y-values greater than the threshold c.
2. Define $\eta(b) := \arg\min_{c \in \mathbb{R}} \left| \sum_{i:x_i > b} p_i - \sum_{j:y_j > c} q_j \right|$. In words, given a threshold b for the vector x, find the c-threshold for the vector y with the property that the volume of $Y(c)$ is closest to $X(b)$. We have denoted this special c, which minimizes the difference between the volume of $X(b)$ and $Y(c)$, by $\eta(b)$. For consistency reasons, we insist that $\mathrm{vol}(A_t) = \mathrm{vol}(A_{t+\tau})$.
3. Starting from $b = \max_i x_i$, we iteratively decrease b, stopping when $\sum_{i:x_i > b} p_i$ becomes greater than some predefined fraction $f \in (0, 1)$. As $X(b)$ grows, so does $Y(\eta(b))$. For each b value we compute $\rho(X(b), Y(\eta(b)))$. The reason for requiring $\mathrm{vol}(X(b))/\mathrm{vol}(X) \leqslant f < 1$ is that if we let $b < \min_i x_i$, then $X(b) = X$, $Y(\eta(b)) = Y$, and $\rho(X(b), Y(\eta(b))) = 1$, which is a trivial result. The purpose of f is to limit the fractional volume of X that $X(b)$ can occupy, and in practice may be usefully set between 1/2 and 1.

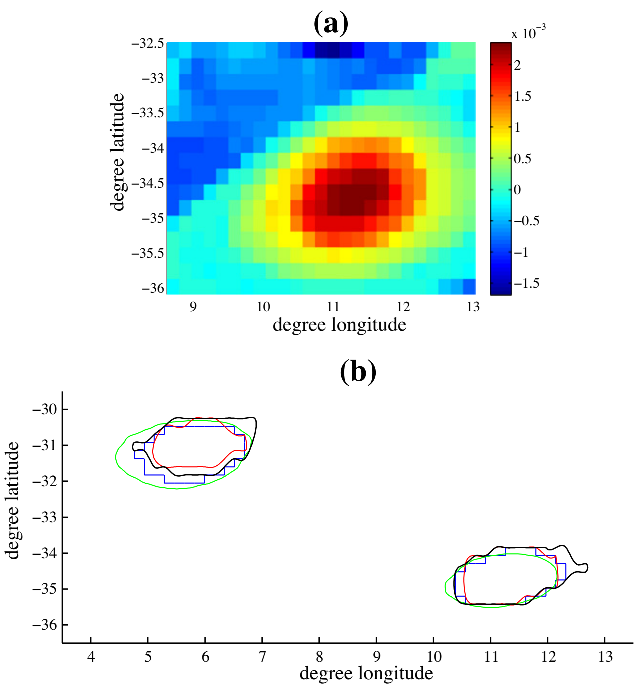

Fig. 2. (a) Surface slice of the vector x. The Agulhas Ring at May 2000 is characterized by high positive values of x. (b) Surface extension of the sets A_{May} and A_{November} (blue) and the boundary of the corresponding structures given by the maximal SSH gradient (green), Okubo-Weiss parameter thresholded by 0.2 times the standard deviation (red) and relative vorticity thresholded by 0.2 times the maximum RV (black). (For interpretation of the references to colour in this figure legend, the reader is referred to the web version of this article.)

4. Repeat Step 3 replacing x and y with $-x$ and $-y$. We now "grow" the set $X(b)$ by thresholding from "the other ends" of x and y.
5. Let b^* be the value of b that maximizes $\rho(X(b), Y(\eta(b))$ from Steps 3 and 4. We set $A_t = X(b^*)$ and $A_{t+\tau} = Y(\eta(b^*))$.

4. Investigation of a single Agulhas Ring

4.1. Three-dimensional characterization

4.1.1. The configuration retained to analyze on Agulhas Ring

The initial domain X is subdivided into a collection of 13,359 boxes such that each box has a side-length of 0.1758° longitude and 0.2246° latitude. The ratio between the longitude and latitude side-length is chosen in such a way that the boxes are approximately square on the surface of the ocean and the vertical extension of the boxes corresponds to the 46 non-uniform depth layers of the ORCA025 model. We filled each box with 216 Lagrangian particles.

We focus on a single Agulhas Ring over the time period mid-May to mid-November 2000. The investigated time period has been chosen for both computational efficiency and oceanographic reasons. Six months is a sufficient period for Agulhas Rings to undergo substantial decay and it is very close to the average lifetime of mesoscale eddies in the global ocean (Chelton et al., 2011). A more detailed discussion can be found in Section 4.1.2.

As the retroflection zone is dynamically very turbulent, we must be careful about the integration step size and the number of test-points for the approximation of (4). If we choose too few test-points over the integration time of 6 months, the final points will not represent the image of the initial boxes well. To avoid this problem, we approximate the transition matrix $\mathbf{P}_{\text{May},6}$ over 6 months by the product $\hat{\mathbf{P}}_{\text{May},6} = \mathbf{P}_{\text{May},1} \cdot \mathbf{P}_{\text{June},1} \cdot \ldots \cdot \mathbf{P}_{\text{October},1}$ of transition matrices over 1 month each. A flow duration of 1 month is sufficiently short that the 216 initial test points in each box flow to a collection that well-represents the true 1-month-image of the box. As a side-effect, by approximating the single transition matrices over shorter time-intervals separately, we add more numerical diffusion due to the box covering. The idea of computing eigenvalues and vectors of a product of two matrices without calculating the product explicit is not new (Varga, 1962) and has been used in a variety of applications i.e. the computation of singular values and vectors.

The magnitude of the singular values represent the coherence of structures given by the thresholding process. The right and left singular vectors corresponding to the second largest singular value, which indicates the strongest coherent structure, shows us a stratification of the state space. This stratification is due to a high discrepancy between horizontal and vertical velocities and leads to dynamical robust structures on each vertical layer. Lower singular values indicated a structure between the surface and 750 m depth and we focused on the region above 750 m depth; the top five singular values are $s_1 = 1$, $s_2 = 0.96$, $s_3 = 0.86$, $s_4 = 0.82$, $s_5 = 0.80$. The surface of the left singular vector corresponding to the 4th singular value, which indicates clearly the Agulhas Ring, is shown in Fig. 2(a).

We proceed by thresholding the singular vector, as described at the end of Section 3, and we end up with two sets A_{May} and A_{November}.

Fig. 3 shows a three-dimensional view of A_{May}. The coherence ratio is 0.7631, which means that 76.3% of the water mass from A_{May} flows into the set A_{November} over 6 months. To visualize the leakage of water of A_{May} after 6 months, we define a vector $v \in \mathbb{R}^m$, which has uniform non-zero entries v_i if $B_i \subset A_{\text{May}}$ and $v_i = 0$ otherwise, and multiply it by $\hat{\mathbf{P}}_{\text{May},6}$. The result,

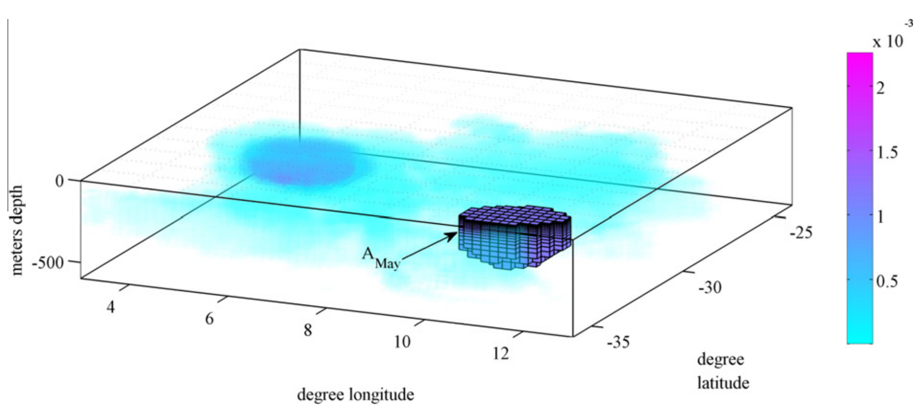

Fig. 3. The initial set (A_{May}) of the detected coherent pair and the final state of an initial density after 6 months. The transparency reflects the concentration of the final density.

$w = v\hat{\mathbf{P}}_{\text{May},6}$, is plotted in Fig. 3, where high values denote a high concentration of mass. This visualization of the distribution of mass starting in A_{May} shows a pathway of water escaping North-Eastwards from the Ring and also demonstrates that most of the mass remains coherent after 6 months.

4.1.2. Parameters and sensitivity analysis

In this section, the sensitivity of our results to changes of some parameters of the technique is tested. We have calculated the singular vectors and values corresponding to $\mathbf{P}_{\text{May},1}$ and $\hat{\mathbf{P}}_{\text{May},3} = \mathbf{P}_{\text{May},1} \cdot \mathbf{P}_{\text{June},1} \cdot \mathbf{P}_{\text{July},1}$, respectively to check the robustness of the choice of the parameter τ for one and three months. The 1−month analysis is displayed in Fig. 4(a) and (b) where (a) shows the surface slice of the normalized left singular vector indicating the Agulhas Ring and (b) shows the thresholded Ring and Fig. 4(c) and (d) show similar results for the investigation over three months. Both 1-month and 3-months flows identify initial coherent structures that are similar to the 6-months flow results shown in Figs. 2(a) and 3, indicating that the transfer operator (or transition matrix) approach is reasonably robust with respect to flow time.

Additionally the sensitivity of the product approach has been investigated using different temporal subdivisions. We have also chosen 12 transition matrices over half a 1-month each and two matrices over 3-months each. The singular vectors indicate very similar structures, attesting of the robustness of our method.

4.2. Surface characterization: a comparative study

To benchmark these identified structures we compare our results with three standard techniques used in the detection of Agulhas Rings, based on Sea Surface Height (SSH), the relative vorticity criterium (RV) and the Okubo-Weiss parameter (OW). These techniques have been developed for the detection of eddies in the ocean surface. In our investigation we also analyze the three-dimensional shape of an Agulhas Ring and therefore extend the surface techniques along the vertical direction for comparison. The surface boundary of A_{May} and A_{November} is shown in Fig. 2(b). It also shows the ring edge as defined by the other techniques i.e. maximum SSH gradient, RV and OW. For the calculation we used the 5-day averaged data on May 1st and the average of the last 5-days in October, respectively. Let $u(x,y)$ and $v(x,y)$ be the velocity of a particle (x,y) on the surface in longitude and latitude direction, respectively. RV is given by $\text{RV}(x,y) = \frac{\partial v}{\partial x} - \frac{\partial u}{\partial y}$ and the OW parameter by $\text{OW}(x,y) = \left(\frac{\partial u}{\partial x} - \frac{\partial v}{\partial y}\right)^2 + \left(\frac{\partial v}{\partial x} + \frac{\partial u}{\partial y}\right)^2 + \text{RV}(x,y)^2$. The calculation of the RV and the OW parameter is done after interpolation of the advection field onto the same grid as the transfer operators. We use a commonly used threshold coefficient to define the edge of the rings, where RV is 0.2 times the maximum RV value at the surface and OW is 0.2 times the standard deviation of OW at the surface (Chaigneau et al., 2008). Fig. 2(b) demonstrates that the different techniques identify similar surface structures.

4.3. Comparison of coherence ratios

To examine the coherence of the three-dimensional structures defined using these techniques, we extend the surface shape down to the depth where the set A_{May} ends (i.e. approx. 300 m). We calculated the OW and RV field for May and November 2000 at each depth level within our box discretization $\{B_1, \ldots, B_m\}$. We use a

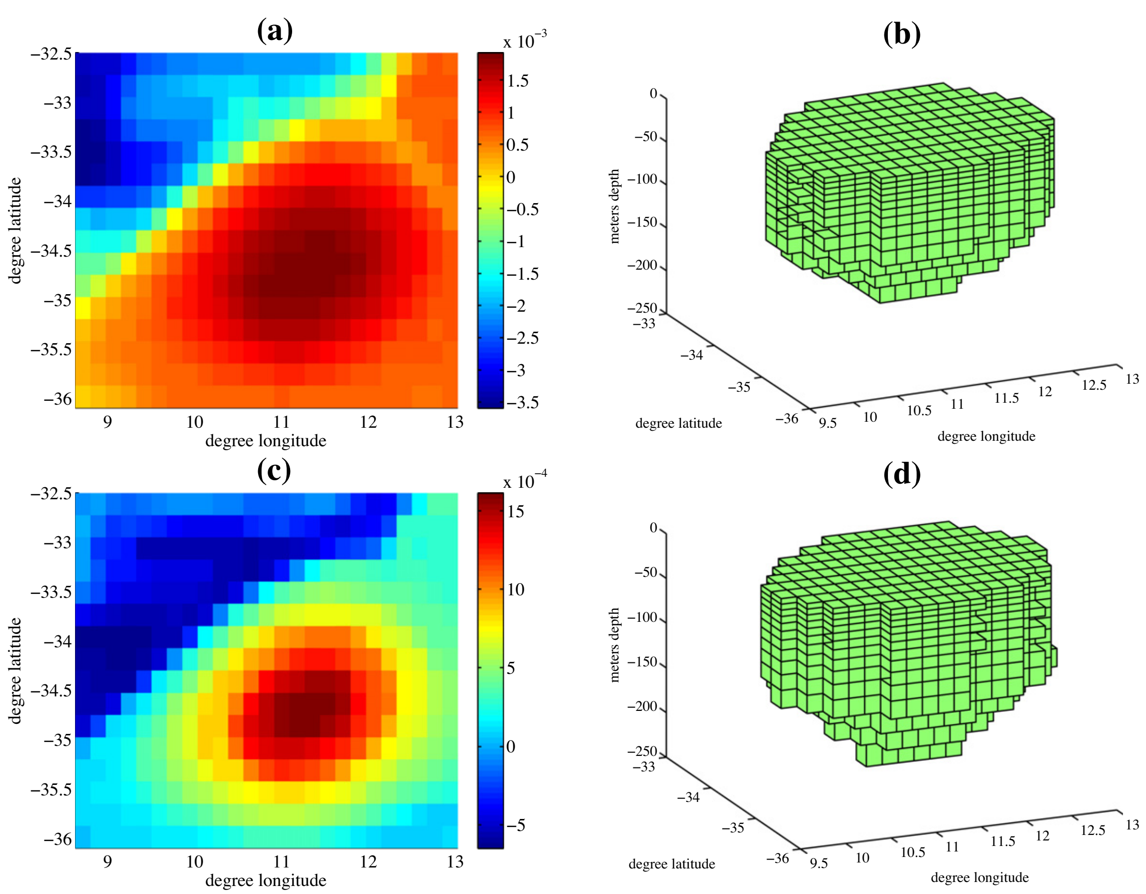

Fig. 4. (a) Surface slice of the normalized left singular vector of the one month analysis indicating the Agulhas Ring at May 2000. (b) The initial set of the detected coherent pair over 1 month. (c) Surface slice of the normalized left singular vector of the three month analysis indicating the Agulhas Ring at May 2000. (d) The initial set of the detected coherent pair over 3 months.

Table 1
Coherence ratios of three-dimensional Agulhas Ring characterization by different techniques.

	Method	Volume	Coherence ratio (%)
1	Transfer operator approach	5481 km^3	76.31
2	OW (0.2 threshold)	7752 km^3	52.17
3	RV (0.2 threshold)	9547 km^3	61.23
4	OW (fitted volume)	5495 km^3	60.87
5	RV (fitted volume)	5492 km^3	61.65
6	OW (optimized threshold)	5527 km^3	60.98
7	RV (optimized threshold)	5693 km^3	62.30

commonly used threshold value of 0.2 for the initial time (for both RV and OW) and scale the threshold for the final time so that the initial and final structures have equal volumes. This is required for consistency of the coherence calculation; for example, if a ring is allowed to grow or shrink, it is difficult to distinguish shrinkage from dissipation. For the three-dimensional study we have chosen two options.

1. We use the same threshold for both RV and OW at the initial time on each level defined for the surface analysis (layer by surface).
2. We calculate the maximal RV and the standard deviation of the OW parameter on each layer separately (layer by layer).

The layer by surface and layer by layer calculations of OW and RV gave identical coherence ratios and we therefore report only the layer by surface results which are shown in line two and three of Table 1.

The transfer operator approach resulted an improvement in the coherence ratio by 15–24% over the other methods. However, the 0.2 threshold results in structures of quite different volumes (Table 1). As such the transfer operator method might just be identifying a smaller core region of the Ring that is more coherent than the larger structures identified by the RV and OW methods. To test this we adjusted the OW and RV thresholds so that the volumes of the structures were almost identical to that identified by the transfer operator approach. While this improved the coherence ratio for the OW method it made little difference in the case of the RV method. The transfer operator method still represents an improvement of approximately 15% over the other methods. We also thresholded both RV and OW by maximizing the coherence ratio which leads to almost the same coherence ratios (62.3% and 60.98%, respectively) as using the fitted volume approach. This shows the ability of the transfer operator approach to identify structures, which evolve coherently over time, within the oceanic flow. The boundaries determined by the transfer operator method define 3D objects that have a greater coherence than the corresponding objects identified by RV and OW; thus, the former are arguably better representations of the eddy. The reasons for this improvement in coherence are that the RV and OW are essentially two-dimensional techniques extended to three-dimensions, and that the transfer operator method is designed to directly capture regions of maximal coherence. Clearly, the accurate delimiting of eddies is crucial to subsequent oceanographic calculations of eddy-induced transport.

5. Conclusions

Agulhas leakage plays an important role in the climate system, acting as a mechanism for transporting heat and salt between basins and closing the large scale overturning circulation. As a result of global climate change there is an expectation that the leakage may change, constituting a feedback onto the large-scale climate (Biastoch et al., 2008; Rouault et al., 2009). The ability to accurately quantify the inter-basin transport and the subsequent decay of rings and other coherent structures is of considerable importance. The leakage of the Agulhas system is in part effected by water transported within the Agulhas Rings. We have demonstrated that we can capture the coherence of a single Agulhas Ring more accurately than other techniques based on surface anomalies. In particular, three-dimensional structures identified using our method were about 15% more coherent than estimates obtained from two other commonly used techniques. This suggests that the most energetic rings may in fact remain coherent for longer than previously thought.

In the future, we will apply our technique to several Agulhas Rings and to other pertinent coherent structures over longer time-intervals. An extension of this work is to follow a similar approach as Chelton et al. (2011) to obtain a parameter-free technique that could be applied to the global ocean. It will allow us to quantify the leakage of the whole Agulhas system and to quantify more accurately how these structures decay with time in a three-dimensional framework.

Acknowledgments

GF is partially supported by the ARC Discovery Project (DP110100068) and GF and CH are partially supported by the 2011/12 Go8/DAAD Australia – Germany Joint Research Co-Operation Scheme. VR is supported by an ARC Grant (DP1093510). We would like to thank two anonymous reviewers and Stephen Griffies for their invaluable and extensive set of comments and suggestions.

References

Barnier, B., Madec, G., Penduff, T., Molines, J.-M., Treguier, A.-M., Le Sommer, J., Beckmann, A., Biastoch, A., Böning, C., Dengg, J., Derval, C., Durand, E., Gulev, S., Remy, E., Talandier, C., Theeten, S., Maltrud, M., McClean, J., De Cuevas, B., 2006. Impact of partial steps and momentum advection schemes in a global ocean circulation model at eddy-permitting resolution. Ocean Dynam. 5–6, 543–567.

Beal, L.M., De Ruijter, W.P.M., Biastoch, A., Zahn, R., 2011. On the role of the agulhas system in ocean circulation and climate. Nature 472 (7344), 429–436.

Biastoch, A., Boning, C.W., Lutjeharms, J.R.E., 2008. Agulhas leakage dynamics affects decadal variability in atlantic overturning circulation. Nature 456 (7221), 489–492.

Byrne, D.A., Gordon, A.L., Haxby, W.F., 1995. Agulhas eddies: a synoptic view using geosat erm data. J. Phys. Oceanogr. 25 (5), 902–917.

Chaigneau, A., Gizolme, A., Grados, C., 2008. Mesoscale eddies off peru in altimeter records: identification algorithms and eddy spatio-temporal patterns. Prog. Oceanogr. 79 (2–4), 106–119, the Northern Humboldt Current System: Ocean Dynamics, Ecosystem Processes, and Fisheries.

Chelton, D.B., Schlax, M.G., Samelson, R.M., 2011. Global observations of nonlinear mesoscale eddies. Prog. Oceanogr. 91 (2), 167–216. http://dx.doi.org/10.1016/j.pocean.2011.01.002.

De Ruijter, W.P.M., Biastoch, L.A., Drijfhout, S.S., Lutjeharms, J.R.E., Matano, R.P., Weijer, W., 1999. Indian–Atlantic inter-ocean exchange: dynamics, estimation and impact. J. Geophys. Res. 104 (C9), 20,885–20,910.

de Steur, L., van Leeuwen, P.J., Drijfhout, S.S., 2004. Tracer leakage from modeled Agulhas Rings. J. Phys. Oceanogr. 34 (6), 1387–1399.

Dellnitz, M., Froyland, G., Horenkamp, C., Padberg-Gehle, K., Sen Gupta, A., 2009. Seasonal variability of the subpolar gyres in the southern ocean: a numerical investigation based on transfer operators. Nonlinear Proc. Geophys. 16, 655–664.

Doglioli, A.M., Blanke, B., Speich, S., Lapeyre, G., 2007. Tracking coherent structures in a regional ocean model with wavelet analysis: application to cape basin eddies. J. Geophys. Res. 112 (C5).

Doglioli, A.M., Veneziani, M., Blanke, B., Speich, S., Griffa, A., 2006. A Lagrangian analysis of the Indian–Atlantic interocean exchange in a regional model. Geophys. Res. Lett. 33 (14).

Froyland, G., Padberg, K., England, M., Treguier, A.M., 2007. Detection of coherent oceanic structures via transfer operators. Phys. Rev. Lett. 98 (224503).

Froyland, G., Schwalb, M., Padberg, K., Dellnitz, M., 2008. A transfer operator based numerical investigation of coherent structures in three-dimensional southern ocean circulation. In: Proceedings of the 2008 International Symposium on Nonlinear Theory and Its Application, Budapest, pp. 313–316.

Froyland, G., Santitissadeekorn, N., Monahan, A., 2010. Transport in time-dependent dynamical systems: finite-time coherent sets. Chaos 20 (4), 043116.

Isern-Fontanet, J., García-Ladona, E., Font, J., 2003. Identification of marine eddies from altimetric maps. J. Atmos. Oceanic Technol. 20 (5), 772–778.

Lutjeharms, J.R.E., 2006. The Agulhas current retroflection. The Agulhas Current. Springer, Berlin, Heidelberg, pp. 151–207.
Morrow, R., Birol, F., Griffin, D., Sudre, J., 2004. Divergent pathways of cyclonic and anti-cyclonic ocean eddies. Geophys. Res. Lett. 31.
Richardson, P.L., 2007. Agulhas leakage into the atlantic estimated with subsurface floats and surface drifters. Deep-Sea Res. Part I 54 (8), 1361–1389.
Rouault, M., Penven, P., Pohl, B., 2009. Warming in the Agulhas current system since the 1980s. Geophys. Res. Lett. 36 (12).
Sadarjoen, I.A., Post, F.H., 2000. Detection, quantification, and tracking of vortices using streamline geometry. Comput. Graphics 24 (3), 333–341.
Schouten, M.W., de Ruijter, W.P.M., van Leeuwen, P.J., Lutjeharms, J.R.E., 2000. Translation, decay and splitting of agulhas rings in the South Eastern Atlantic ocean. J. Geophys. Res. 105 (C9), 21,913–21,925.
Treguier, A.M., Boebel, O., Barnier, B., Madec, G., 2003. Agulhas eddy fluxes in a 1/6° Atlantic model. Deep-Sea Res. Part II 50 (1), 251–280, inter-ocean exchange around Southern Africa.
van Aken, H.M., van Veldhoven, A.K., Veth, C., de Ruijter, W.P.M., van Leeuwen, P.J., Drijfhout, S.S., Whittle, C.P., Rouault, M., 2003. Observations of a young Agulhas Ring, astrid, during mare in March 2000. Deep-Sea Res. Part II 50 (1), 167–195.
van Sebille, E., van Leeuwen, P.J., Biastoch, A., de Ruijter, W.P.M., 2010. On the fast decay of Agulhas Rings. J. Geophys. Res. 115 (C3).
Varga, R.S., 1962. Matrix Iterative Analysis. Prentice-Hall Inc., Englewood Cliffs, NJ (xiii+322 pp.).
Weijer, W., Ruijter, W.P.M.D., Sterl, A., Drijfhout, S.S., 2002. Response of the atlantic overturning circulation to South Atlantic sources of buoyancy. Global Planet. Change 34 (3–4), 293–311.